

# Enhancing Lithium-Ion Battery Performance with Alumina-Coated Separators: Exploring the Potential of Different Alumina Particle Sizes, Coating Techniques, and Calendering

Meisam Hasanpoor,<sup>[a]</sup> Robert Kerr,<sup>[a]</sup> Maria Forsyth,<sup>[a]</sup> and Patrick C. Howlett<sup>[a]</sup>

A range of techniques for the coating of high purity alumina (HPA) on porous polypropylene battery separators has been investigated. A slurry was prepared by dispersion of the alumina powder in acetone solvent and poly (vinylidene fluoride-co-hexafluoropropylene) (PVdF-HFP) as the binder to obtain an excellent adhesion to the membrane. Doctor blade, spin coating, and electro-spin coating techniques were utilized to coat a thin layer of HPA on the separator that was followed up with a calendering step to improve compactness, decrease thickness

and enhance adhesion. Furthermore, the effect of HPA particle size, distribution, and the use of a calendering step on coating thickness, compactness, and electrochemical performance were investigated using three HPA sources. The doctor blade technique was found to give the most uniform coating with the best mechanical properties and high-temperature resistance. The coated separators were incorporated into lithium-ion coin cells to evaluate the rate capability and long-term cycling performance.

## Introduction

Ceramic-coated membranes are increasingly popular in various applications due to their high stability, temperature resistance, and improved separation performance. They are used in water treatment, food and beverage, pharmaceuticals, gas separation, and energy applications.<sup>[1,2]</sup> Among them, alumina-coated membranes are beneficial due to their high surface area, chemical and mechanical stability, improved mechanical properties, and enhanced surface properties.<sup>[3]</sup> Alumina coatings can effectively, improve durability, reduce fouling, and enhance separation performance in different applications.<sup>[4]</sup>

One of the main application targets of the alumina coated membranes is incorporating them within lithium-ion batteries (LIBs) as a separator. LIBs are widely considered the most promising energy storage technology due to their high energy density, long cycle life, and superior rate performance. With the increasing demand for electric vehicles and other forms of electrified transportation, researchers are working to improve the cell components and achieve long lasting performance across a wide range of temperatures.

One key area of concern in LIBs is battery safety, particularly the puncture strength and thermal stability of the separator. These separators are critical components that prevent the electrodes from coming into physical contact while still

allowing ions to pass through.<sup>[5]</sup> Commercial separators are typically made of chemically stable, porous polymer layers or non-woven mats. The use of microporous separators is common in lithium-ion batteries. However, there are concerns about the failure of these membranes at high temperatures due to curling and shrinkage, especially above 50 °C.<sup>[6,7]</sup> Moreover, separators are known to be the main limiting factor for heat dissipation within the battery because of their low thermal conductivity.<sup>[8]</sup> Therefore, it is crucial to develop separators that have high thermal stability, conductivity, and electrolyte wettability to enhance the safety and performance of LIBs.<sup>[9]</sup>

Numerous studies have been conducted to tackle the problem of thermal stability and electrolyte wettability by utilizing various coatings, composite fibers, and different inorganic materials.<sup>[10,11]</sup> Passerini and colleagues<sup>[12]</sup> have created stable high-temperature separators using an environmentally friendly manufacturing process. These separators are composed of SiO<sub>2</sub> and hydroxypropyl guar gum and possess high electrolyte uptake and thermal stability. Zhang and colleagues<sup>[13]</sup> have developed a nonwoven composite separator based on cellulose, which has exceptional flame retardation properties, along with good thermal stability and rate performance. Jiang and co-workers<sup>[14]</sup> have created a new type of separator where ceramic particles are grafted onto the polymer material. This innovative separator has high thermal stability and shows negligible shrinkage even at a temperature of 150 °C.

The calendering process is well established in the separator manufacturing process that can improve the mechanical strength and thickness uniformity of the separator, increase its density, and enhance its thermal stability and electrolyte uptake.<sup>[15,16]</sup> Several published studies have demonstrated the effectiveness of calendering in improving the performance and safety of lithium-ion batteries,<sup>[17,18]</sup> however the studies on the ceramic coated separator calendering has been very limited to

[a] M. Hasanpoor, R. Kerr, M. Forsyth, Prof. P. C. Howlett  
Institute for Frontier Materials, Deakin University, 221 Burwood Highway, Burwood, Victoria 3125, Australia  
E-mail: patrick.howlett@deakin.edu.au

© 2024 The Authors. Batteries & Supercaps published by Wiley-VCH GmbH. This is an open access article under the terms of the Creative Commons Attribution Non-Commercial NoDerivs License, which permits use and distribution in any medium, provided the original work is properly cited, the use is non-commercial and no modifications or adaptations are made.

date. For example, a study by Wang et al.<sup>[19]</sup> reported an efficient improvement in the separator pore size and porosity in non-woven separators that could influence the cell performance. More studies are yet to come regarding the impact of calendering on the ceramic coated separators as it can enhance the properties of the separators by compressing and smoothing the coating.

In this study, the impact of several factors, namely the size and morphology of alumina particles, coating technique, and calendering technique on the quality, homogeneity, and cyclability of the coated separator in lithium-ion batteries are explored.

## Experimental Section

### Preparation of the Coated Separator

In this study, high purity alumina (HPA) with various particle size and morphology were used as the main alumina precursors. Moreover, PVdF-HFP (Solvay) with  $M_w \sim 400000$  and acetone (99.9%, Merck) were used as the binder and the solvent, respectively. The coated Celgard 3501 separators were prepared by using below three steps: 1) To prepare a slurry, HPA: PVdF-HFP: Acetone (ratio of 10:1:44 wt%) were mixed under continuous stirring using a hotplate stirrer (IKA-Werke) with a rate of 800 RPM for 5 h at 50°C. 2) To prepare the wet coated separators, three different methods including blade coating, spin coating and electro-spin coating were utilized. Blade coating and Spin coating techniques were applied using 120 µm doctor blade and 500 RPM rotational speed, respectively. Moreover, Electro-spin coating technique was applied using a custom-made facility with a voltage of 10 kV, the distance of 7.5 cm (between nozzle and the separator) and injection speed of 1 ml·min<sup>-1</sup> (Figure 1). 3) To dry the wet coated separators, all the samples were constrained between two flat glasses for 24 h at room temperature. Depending on the chosen technique, the thickness of the as-prepared coated separator varied between 5–30 µm.

### Separator Characterization

Unless stated otherwise, the following measurements were performed at room temperature.

A scanning electron microscope (SEM), JSM-IT300 (JEOL, Japan), was used to observe the particle size and morphology in addition to the surface and cross-sectional morphology of the coated separator.

Mastersizer 2000, a product of Malvern Instruments was used to analyse the particle size distributions of the HPA powders dispersed in distilled water. This technique uses laser diffraction system and is capable of measuring wet and dry powder samples.

Solid-state <sup>27</sup>Al magic angle spinning (MAS) NMR was used to study the crystalline structure of the HPA samples. The samples were packed into 4 mm zirconia MAS rotors. A Bruker Avance III 500 MHz (11.7 T) wide-bore NMR spectrometer equipped with a 4 mm magic angle spinning (MAS) probe was used acquire the <sup>27</sup>Al spectra. Moreover, to study the electrolyte decomposition, the same equipment was used to measure <sup>1</sup>H, <sup>13</sup>C and <sup>19</sup>F NMR and characterize the samples after leaching the custom-coated separator for a month at room temperature. All the data were collected at a MAS rate of 12.5 kHz at room temperature.

A 3D optical profilometer (Bruker, Veeco-Wyko) was employed to image the surface morphology of the separators. The instrument system is based on a noncontact GT-K1 interferometer on a vibration isolation table to avoid any parasitic movements. The green band light source was employed for imaging to reach to a higher magnification and the bundled Vision 64 software was used to analyse the acquired images. In order to obtain a suitable scanning result, automatic image stitching was done to extend the imaging area and obtain high-resolution images at different magnifications.

For the electrolyte uptake experiment, Celgard 3501 separator were punched into 16 mm diameter discs and then were soaked in electrolyte for 15 minutes, and excessive electrolyte on was absorbed and removed using filter paper. The electrolyte uptake calculation was followed using the equation below:

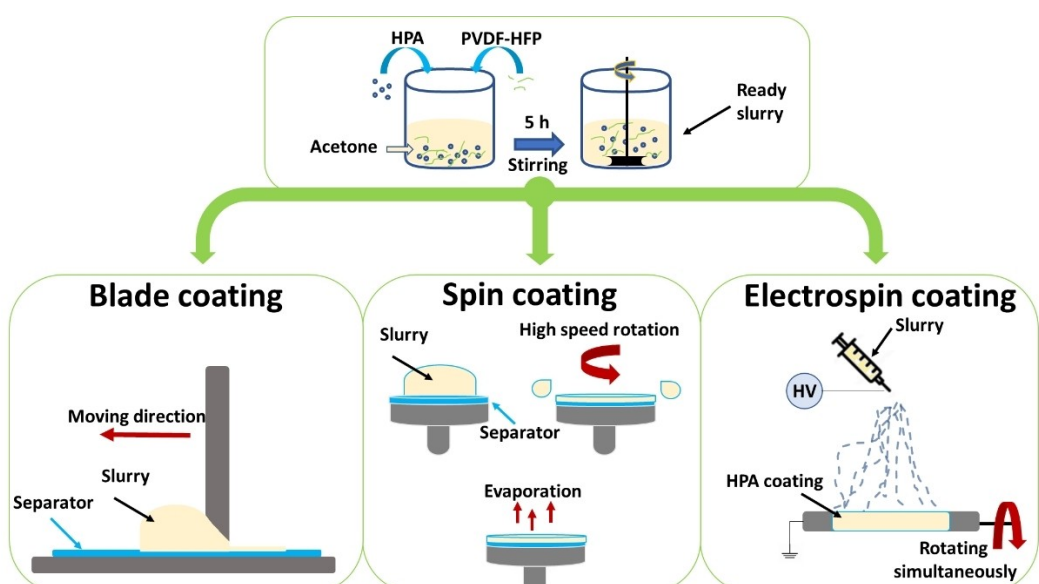


Figure 1. Schematic of HPA-coated separator preparation employing various coating techniques.

$$\text{Electrolyte uptake percentage} = 100 \times (M - M_0) / M_0$$

The weights of the separator discs before and after absorbing electrolyte are denoted as  $M_0$  and  $M$ , respectively. The average values of electrolyte uptake were reported based on the results of three samples.

### Cell Preparation and Cycling

Graphite | NMC811 cells were assembled in coin cells (CR2032) purchased from Hohsen Co (Tokyo, Japan), in an argon glovebox. 10 mm diameter graphite anode ( $2.4 \text{ mAh.cm}^{-2}$ ) and 8 mm diameter  $\text{LiNi}_{0.8}\text{Mn}_{0.1}\text{Co}_{0.1}\text{O}_2$  (NMC811) cathode ( $2 \text{ mAh.cm}^{-2}$ ) purchased from CustomCells, were used in the cells. 70  $\mu\text{l}$  electrolyte (1 M  $\text{LiPF}_6$  in EC:DMC (3:7 wt/wt) + 2% VC) (SOLVIONIC) was used (35  $\mu\text{l}$  on each side) in each cell. A stainless-steel spring has placed in the cell to maintain constant internal pressure ( $1\text{--}2 \text{ kg.cm}^{-2}$ ) and make suitable contact between the cell parts, moreover Graphite electrode was placed on a 1 mm thick, 16 mm diameter stainless steel spacer. All of the cell parts, including the cell components and HPA coated separator (3501 Celgard Inc.), were vacuum dried for 48 h at  $50^\circ\text{C}$  and were kept in an argon-filled glovebox. Moreover, NMC811 cathode and graphite anode were vacuum dried at  $100^\circ\text{C}$  for 24 h prior to assembly.

The prepared cells were stored at room temperature for 24 h before being cycled. A BTS4000 (NEWARE) battery cycler was used for the cell cycling at room temperature to evaluate the rate capability of

the cells in various charging rates of C/5 (5 h charging/discharging time), C/2 (2 h charging/discharging time), 1 C (1 h charging/discharging time), 2 C (30 min charging/discharging time) and 3 C (20 min charging/discharging time).

Electrochemical impedance spectroscopy (EIS) was measured after 100 cycles immediately after the charging step while being held at open circuit voltage (OCV), with spectra recorded from 30 kHz to 1 Hz with a 10 mV amplitude.

## Results and Discussion

### Material Characterization

The SEM analysis on HPA particles, revealed three distinct morphologies as shown in Figure 2. The first type, HPA-1, displayed a close to spherical morphology with a fine particle size and even distribution. The second type, HPA-2, had a porous disk-shape morphology with an uneven distribution of particle size and shape. The milling process resulted in smaller semi-spherical particles with an uneven distribution. Lastly, HPA-3 had significantly larger particle size with a lamellar-cluster morphology that was unevenly distributed in both size and morphology.

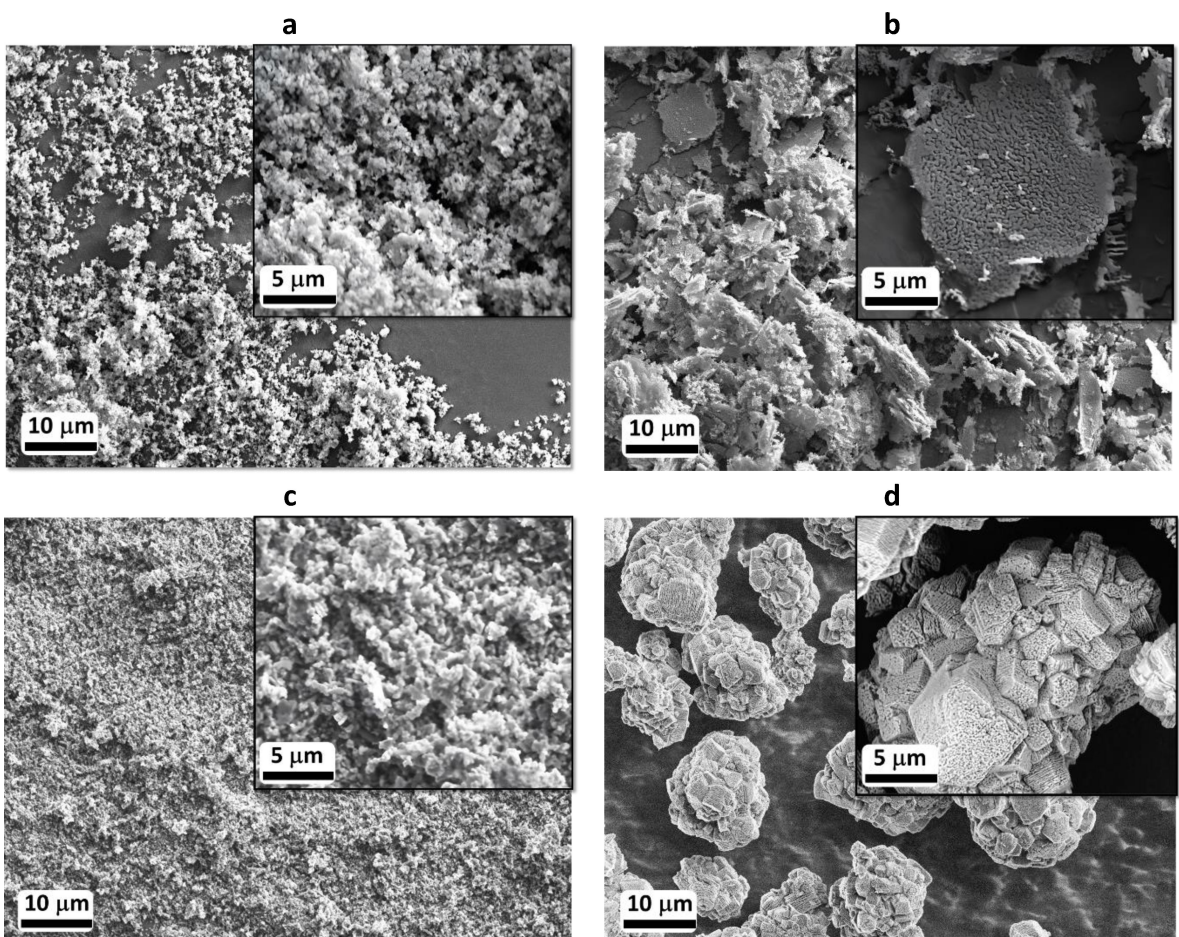
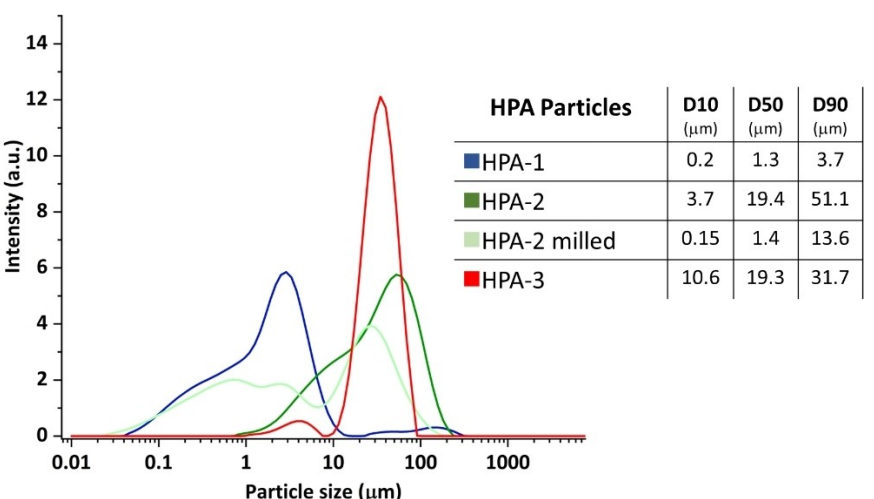


Figure 2. SEM images of the particle size and morphology of a) HPA-1, b) HPA-2, c) HPA-2 milled and d) HPA-3 samples.



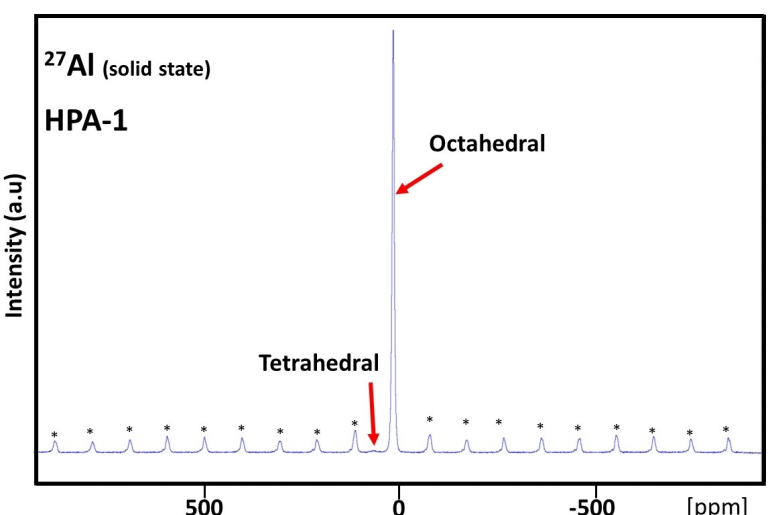
**Figure 3.** Particle size distribution of the HPA powders.

Figure 3 shows the results of a particle size distribution analysis (PSD) of the HPA samples after sonication in distilled water. HPA-1 had the smallest average particle size of around 3  $\mu\text{m}$  with a wide distribution at lower particle sizes. HPA-2 had a wider size range with 90% of particles below 51.1  $\mu\text{m}$  and a distribution starting at 200  $\mu\text{m}$  down to 1  $\mu\text{m}$ . The milling process shifted the distribution to lower values with 90% of particles below 13.6  $\mu\text{m}$ . HPA-3 had a narrow distribution of particles between 10–100  $\mu\text{m}$  with 90% of particles below 31.7  $\mu\text{m}$ .

The crystalline structure of the HPA samples was analysed using solid-state  $^{27}\text{Al}$  MAS NMR, which is an accurate method to examine structural imperfections in alumina (Table 1).<sup>[20,21]</sup> The HPA samples showed variations in the relative amount of two different aluminium coordination environments, quantified by the relative intensities of the two peaks seen in Figure 4. The peak resonance close to 13 ppm indicated the presence of octahedrally coordinated aluminum sites, while the resonance

near 65 ppm is associated with tetrahedral aluminium, most likely arising from the  $\theta$ -alumina phase.<sup>[22]</sup> No  $^{27}\text{Al}$  chemical shift differences were observed in these samples.

Table 1 reveals that all three samples possessed mainly  $\alpha$ -alumina (octahedrally coordinated aluminium with coordination number (CN)=6). The HPA-2 sample had a 100%  $\alpha$ -Alumina (octahedral)(CN=6) crystalline structure with no structural imperfection, whereas HPA-1 had a limited amount of structural imperfection due to the existence of the  $\theta$ -alumina structure (less than 1%) (Table 1). HPA-1's  $\theta$ -alumina content was classified as a low-level crystalline structural imperfection that may have occurred during the manufacturing process. HPA-3 demonstrated a similar but slightly higher level of  $\theta$ -alumina in the structure than HPA-1.



**Figure 4.** Solid state  $^{27}\text{Al}$  MAS NMR spectrum obtained from the HPA-1 sample taken at 25 °C. Spinning sidebands are indicated by asterisks.

**Table 1.** Solid state  $^{27}\text{Al}$  NMR of the HPA samples.

Precursor	Octahedral (CN = 6) (%)	Tetrahedral (CN = 4) (%)	Chemical shift (ppm)
HPA-1	99.1	0.9	13.23
HPA-2	100	–	13.28
HPA-3	98.9	1.1	13.21

## Coating Development

### Slurry Preparation

Achieving a homogeneous coating and maintaining the mechanical properties of the coating is critical in optimizing the slurry for the coating process.<sup>[23]</sup> Table 2 outlines the examined ratios of HPA, binder, and solvent (Acetone) and provides suitable ratios for a proper slurry. In high ratios of HPA powder to the binder (boxes in red), there is a high tendency for HPA powder precipitation, making it difficult to obtain a stable suspension, and has resulted in coatings with unacceptable mechanical properties due to insufficient binder to provide adequate cohesion between the membrane and the coating. However, when using larger HPA particle sizes, a higher binder ratio is recommended to achieve adequate adhesion.

Conversely, low mixture ratios (boxes in orange) increase the likelihood of binder clogging during slurry preparation.

However, they are more likely to provide a stable suspension. A mixture ratio of 6:1 up to 10:1 (HPA powder:binder) is appropriate to obtain a high HPA ratio and avoid HPA powder precipitation and binder clogging (boxes in blue). Coated separators using these ratios have good mechanical properties while containing a high amount of HPA powder in the structure. In summary, the ratio between HPA and binder must be customized based on particle size, morphology, and coating technique. Achieving a stable slurry is essential to obtain a homogenous coating, and optimal mechanical properties.

### Effect of Coating Techniques

In Figure 5, three coating techniques were employed to apply HPA-1 powder onto the Celgard 3501 membrane. For the blade coating, three different slurry loading thickness including 60  $\mu\text{m}$ , 90  $\mu\text{m}$  and 120  $\mu\text{m}$  were applied on the surface. The optimum quality was achieved when 120  $\mu\text{m}$  was used, however the thickness of the coating in the dried sample after evaporation of the solvent is less. Spin coating was conducted applying four major spinning speeds, in which 500, 1000, 2000, and 3000 RPM were examined. An appropriate level of mechanical/morphological coating properties were obtained where 500 RPM was applied. The surface morphology of the coated separators using blade coating and spin coating techniques are similar, whereas the coating compactness varies. On the other hand, the electro-spin coating technique results in

**Table 2.** Mixture ratio (% wt) of HPA powder, PVdF-HFP binder and acetone solvent to prepare the slurries.

Alumina	2	3	4	5	6	8	10	11	12
PVdF-HFP	1	1	1	1	1	1	1	1	1
Acetone	12	16	20	24	28	36	44	48	52
Outcome	Binder clogging					Suitable properties			Poor adhesion

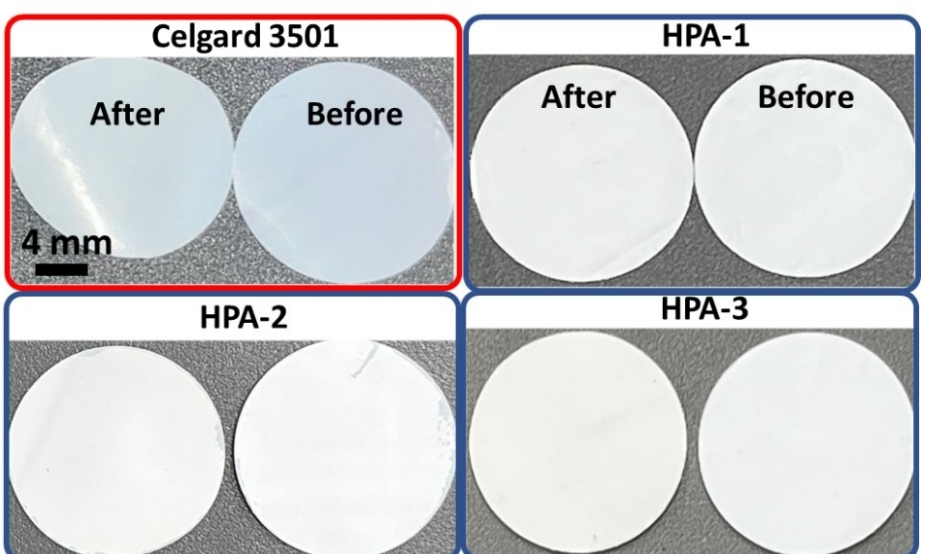


**Figure 6.** Aged Celgard 3501 as a reference without coating at 120 °C for 18 hours, and the HPA coated Celgard 3501 using various particle size and morphology.

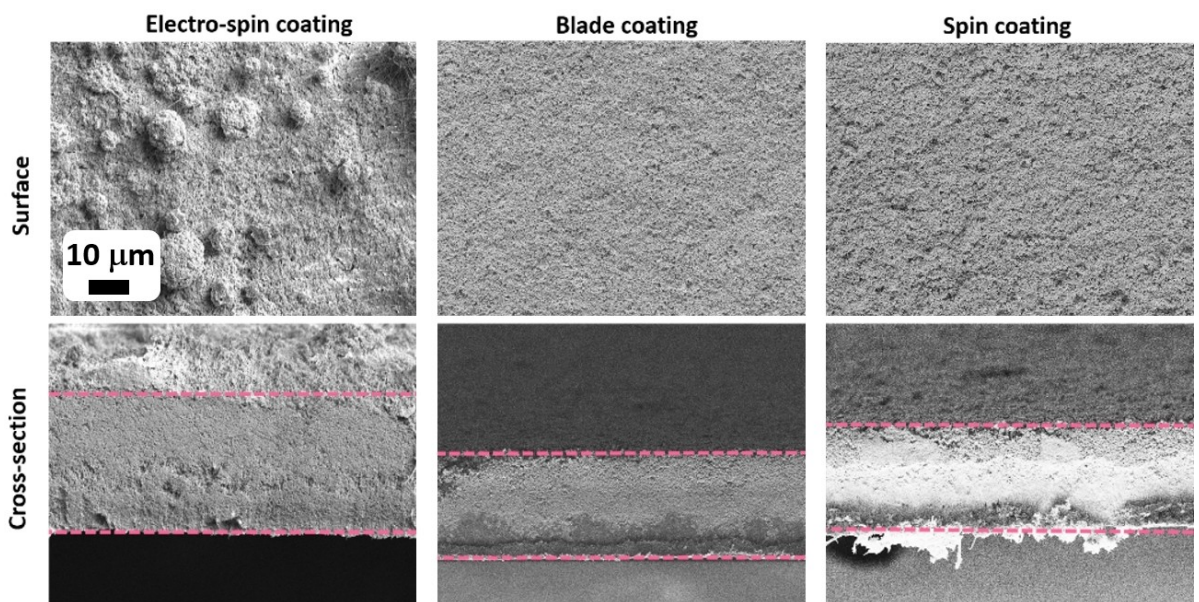


**Figure 5.** SEM images of the surface and cross-sectional morphology of the coated Celgard 3501 employing various techniques using HPA-1: PVdF-HFP: Acetone 10:2:48 wt% as the slurry.

an unfavorable agglomeration of particles on the surface with stranded binder on top. Cross-sectional SEM images provide a better perspective on the coating thickness and surface roughness.

The spin and blade coating techniques appear to be promising candidates as they produce a coating with a smooth surface and a thickness of around 10  $\mu\text{m}$ . In contrast, the electro-spin coating method forms a thicker and jagged coating layer that may negatively affect the membrane properties. Additionally, a digital thickness gauge was utilized as a supplementary method, with careful adjustment to minimize pressure on the flexible separator. The average thickness, based on five measurements, was found to be 34  $\mu\text{m}$  for spin-coated, 38  $\mu\text{m}$  for blade-coated, and 49  $\mu\text{m}$  for electro-spin-coated separators. By adjusting the coating parameters and mixture ratios, the coating thickness and surface morphology can be modified in both blade and spin coating techniques.

In addition, various basic tests were conducted to measure the mechanical strength of coated separators. The preliminary bending test involves bending the coated separator to a certain angle and observing whether the coating cracks or peels off. This test measures the flexibility and adhesion strength of the coating. The crosshatch adhesion test involves making a series of cuts in the coating to form a crosshatch pattern, applying tape to the pattern, and then removing the tape to determine whether the coating adheres strongly to the substrate and assessing visually on scale of 0 to 5. This test measures the strength of the bond between the coating and the substrate.<sup>[24]</sup> Based on the results of these tests, the study found that blade coating exhibited the best mechanical properties, meaning that it was the most resistant to scratches, cracks, and peeling (scale 3 out of 5), and had the strongest bond with the substrate. In contrast, the electrospin coating (5 out of 5) exhibited the poorest behavior, meaning that it was the least

resistant to mechanical stress and had the weakest bond with the substrate.

When selecting a coating method, scalability is an important consideration. Blade coating has already been upscaled and is used for coating batteries' electrodes, therefore it has a greater potential to be utilized on an industrial scale. On the other hand, the spin coating method may be better suited for smaller scales where a customized membrane coating is required. The electrospin coating technique, however, poses additional challenges when optimizing and scaling up, as multiple extra parameters such as applied potential, spin rate, slurry viscosity, and so on which may impact the coating properties. As a result, the blade coating method was chosen as the coating technique for the remainder of the study.

#### Aging StudiesSeparator Thermal Stability

The degradation of separators due to thermal shrinkage at elevated temperatures is mainly observed in membranes with low melting points such as polypropylene (PP) and polyethylene (PE). This shrinkage can lead to changes in pore size and porosity, ultimately causing pore blockage and a compromise in ion mobility and cell performance.<sup>[6,25]</sup> To understand the effect of coating on separator dimensional integrity, a temperature-aging test was conducted in this study. The Celgard 3501 reference sample, which was uncoated, exhibited severe shrinkage after being kept at 120 °C for 18 hours (Figure 6). It is important to note that shrinkage levels are expected to be lower at lower temperatures, but prolonged cycling times can exacerbate the level of shrinkage even at lower temperatures.

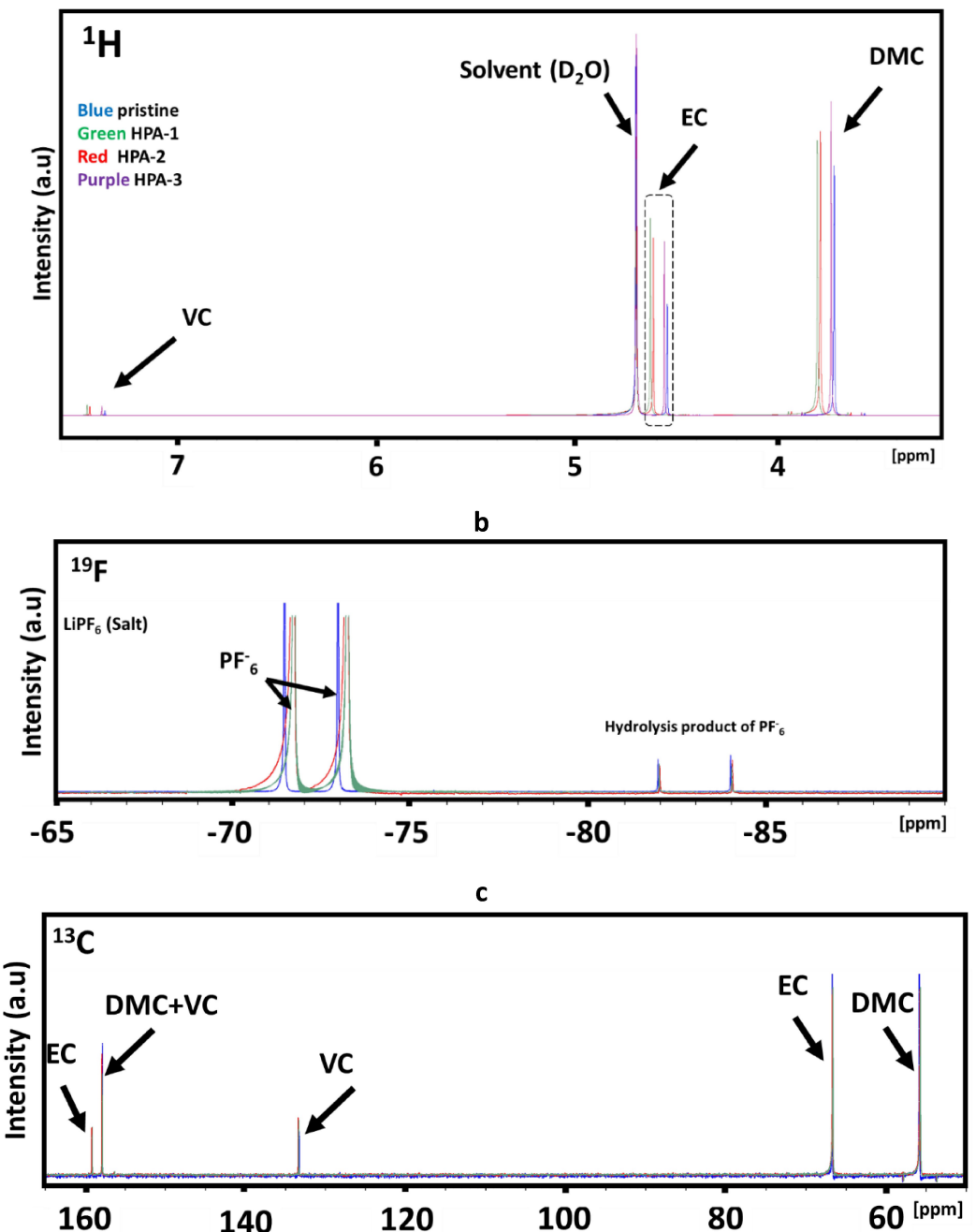


Figure 7. a)  $^1\text{H}$ , b)  $^{19}\text{F}$  and c)  $^{13}\text{C}$  liquid-state NMR spectra of the leached HPA coated membranes in the electrolyte for a month at room temperature.

Fortunately, coating the separator with HPA powders can improve the thermal tolerance of Celgard 3501 and reduce membrane shrinkage to almost zero level. Coated separators can therefore perform better and minimize the risk of thermal runaway in lithium batteries by preventing shrinkage and pore blockage even in harsh environments and heavy-duty applications.<sup>[26]</sup> This improvement in thermal tolerance is especially important for maintaining separator integrity and preserving ion mobility and cell performance in extreme conditions.

#### Electrolyte Decomposition

Liquid-state NMR was used to examine the effects of HPA coating on electrolyte decomposition.  $^1\text{H}$ ,  $^{13}\text{C}$ , and  $^{19}\text{F}$  NMR spectra were recorded to investigate the electrolyte decomposition after the custom-coated samples were soaked in 1 M LiPF<sub>6</sub> in EC: DMC (3:7 wt/wt) + 2% VC electrolyte for one month at room temperature.

The results of the investigation are shown in Figure 7, which depicts the  $^1\text{H}$ ,  $^{13}\text{C}$ , and  $^{19}\text{F}$  NMR spectra of the electrolyte after leaching three coated separators inside 1 ml of electrolyte at room temperature for one month. It

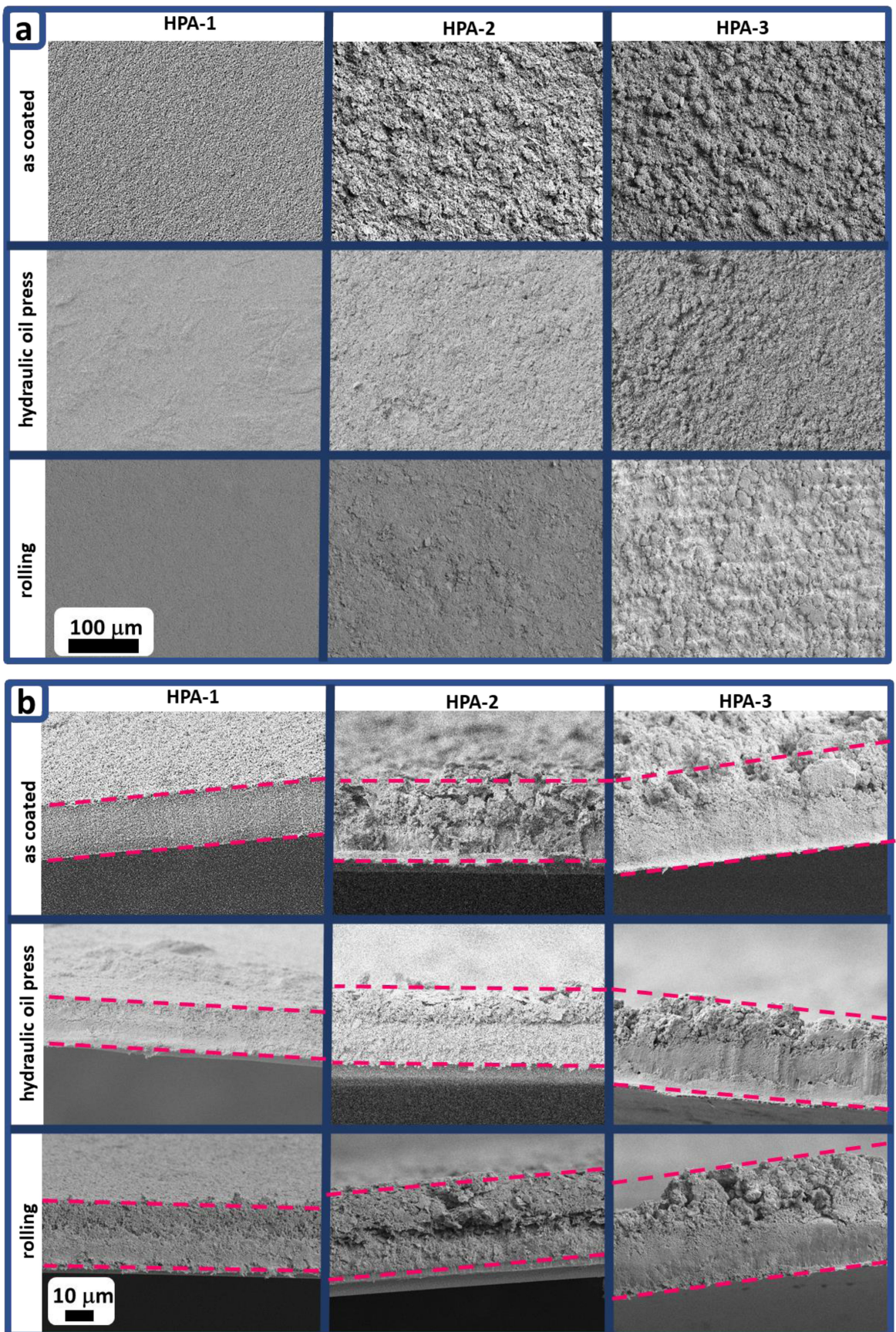
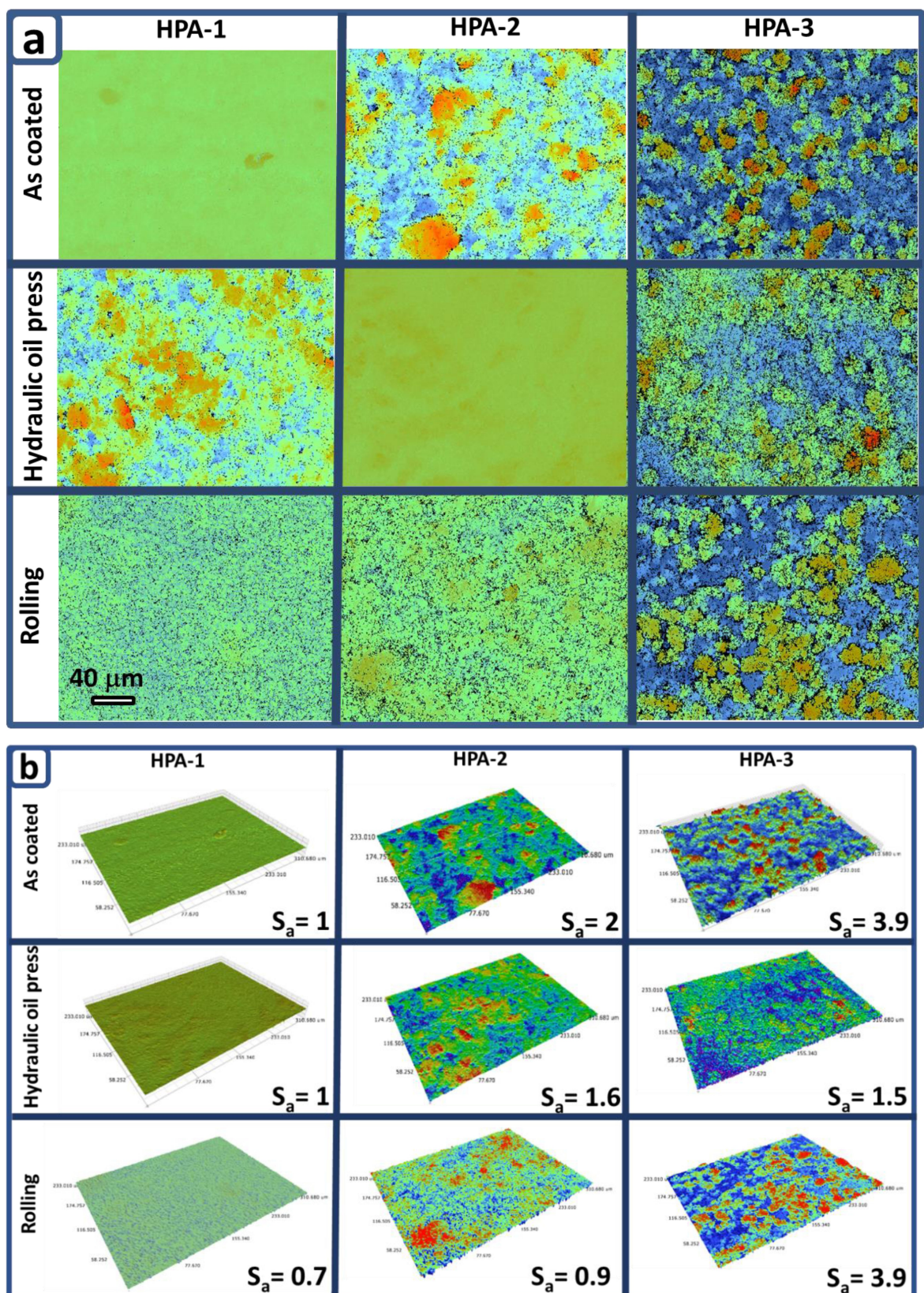
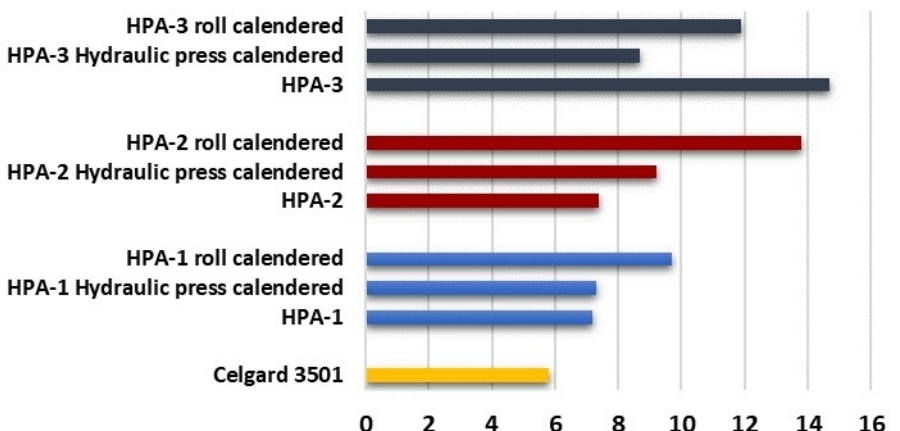


Figure 8. SEM images of the a) surface, and b) cross section of the non-calendered and calendered samples using various HPA precursors.



**Figure 9.** a) 2D, and b) 3D images obtained from the surface of the non-calendered and calendered samples employing an optical profilometer using various precursors. ( $S_a$  indicates the surface roughness).

## Electrolyte uptake (mg)



**Figure 10.** Electrolyte uptake of the coated and calendered separators employing various HPA particles in the electrolyte of 1 M LiPF<sub>6</sub> in EC:DMC (3:7 wt/wt) + 2% VC.

should be noted that visual tests of the electrolyte after the leaching process revealed no change in color and no detachment or dispersion of the coating particles within the electrolyte. Additionally, no new peaks are observed in the spectra, indicating the high stability of the electrolyte during the test and its resistance to decomposition when in contact with the coated separator over time. As a result, HPA-coated separators do not induce or accelerate any parasitic reactions that could lead to electrolyte decomposition while soaking in the electrolyte. However, some minor peak shifts for the organic solvent molecules and PF<sub>6</sub><sup>-</sup> anions are observed after the leaching process, in the <sup>1</sup>H and <sup>19</sup>F spectra which may be attributed to the detachment and dissolution of a small amount of HPA (either as Al<sup>3+</sup> ions or small particles) and/or PVdF-HFP binder into the electrolyte.

To further investigate this phenomenon, <sup>27</sup>Al spectra were also acquired from the leached electrolyte, but no peak was detected, suggesting that any detachment and dissolution of HPA occurs at a very low concentration. Therefore, it can be concluded that the HPA-coated separators have a minimal impact on the stability of the electrolyte, and they are unlikely to cause any significant degradation of the electrolyte over time.

### Calendering

Calendering involves compressing the dried coated separator to reduce porosity, improve particle compactness, and enhance mechanical properties.<sup>[27]</sup> Modifying the coating structure through calendering can improve the mobility of ions in LIBs,<sup>[28]</sup> which can result in optimal energy or power density. However, as porous separators are made of formable polymers that are sensitive to pressure and temperature, the calendering process can compromise their

mechanical properties by changing their dimensions, pore size, and structure.<sup>[7,29]</sup> Therefore, this study aimed to determine the optimum conditions for calendering to achieve optimal coating porosity, particle compactness, and avoid detrimental deformation, delamination, and mechanical damage on the custom-coated separators.

To determine the optimal calendering conditions, various time, pressure, and temperature were examined using hydraulic press and roll calendering techniques. The results showed that applying 1 tonne/m<sup>2</sup> at room temperature for 30 minutes provides the best calendering when using the hydraulic press calendering technique. On the other hand, the roll calendering technique requires rolling the coated separator in between rolls with 5–8 µm less thickness than the coated sample (depending on the HPA particle size and morphology) to achieve a homogenous surface finishing and proper compactness.

Figure 8 illustrates the scanning electron microscopy (SEM) images of the surface and cross-section of the coated separator before and after calendering with various HPA precursors. The results show that calendering significantly affects the surface morphology, roughness, and compactness of the HPA coating. The surface of the calendered samples appears to have less inhomogeneity and more even distribution of particles, particularly in the case of HPA-2 and HPA-3 samples due to their larger particle size and morphology, which leads to larger gaps between particles and higher porosity in the coating. Additionally, the cross-sectional SEM images indicate that the coating porosity has been reduced and the particle arrangement has been optimized, which could result in better compactness, thinner coating, and improved coating adhesion. It should be noted that the coating pores accommodate the electrolyte and directly affects the charge transport, ion mobility, and membrane wettability. Larger particles with coarse aggregate morphology could further amplify this effect.<sup>[30]</sup>

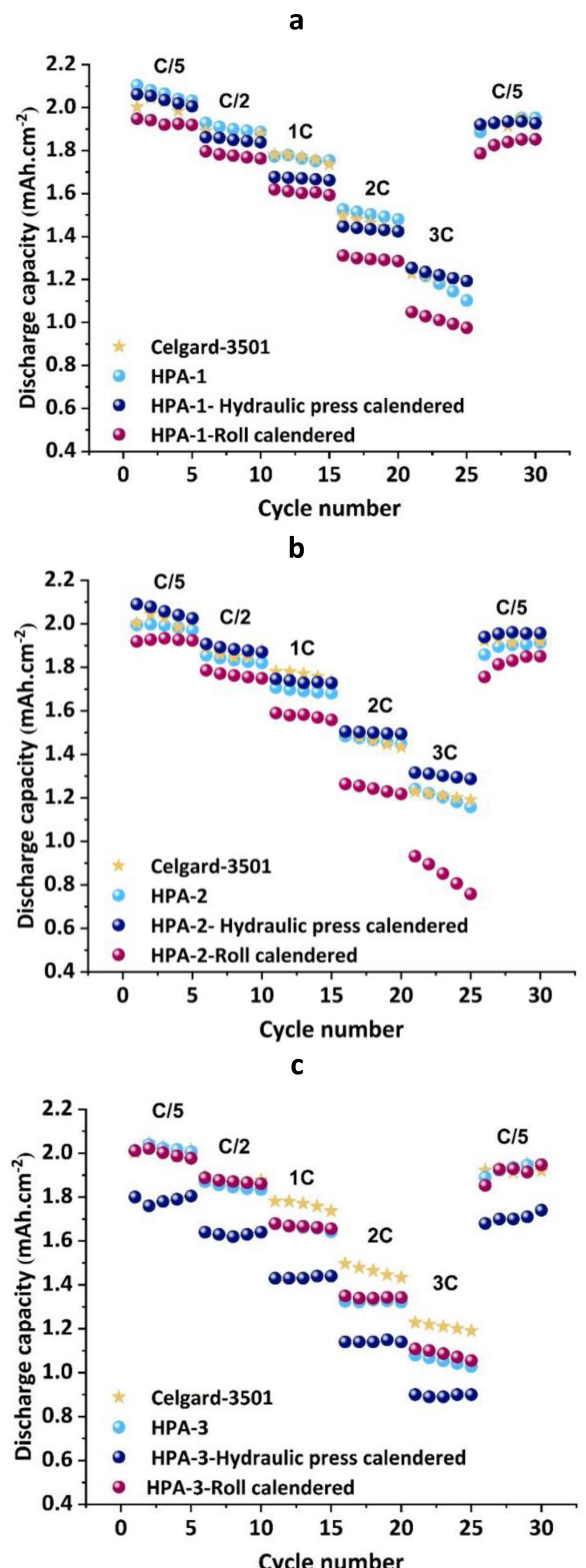


Figure 11. Rate capability of  $\text{Gr} \parallel \text{NMC811}$  ( $2 \text{ mAh.cm}^{-2}$ ) full cells under various calendering techniques for a) HPA-1, b) HPA-2, and c) HPA-3.

Therefore, any changes in the coating porosity and compactness will inevitably impact the overall separator performance.<sup>[31]</sup>

Figure 9 exhibits 3D and 2D images obtained using an optical profilometer to analyze the surface of the coated separator before and after calendering using precursors in different sizes and morphologies. The optical profilometer is a reliable tool that can accurately visualize the surface roughness and morphology of coated samples, enabling a better understanding of particle arrangement on the surface.<sup>[32]</sup> However, this technique solely provides information regarding the coating surface and not the coating porosity and structure. Therefore, a combination of SEM and 3D profilometer studies can be utilized to accurately characterize the coating structure.

The results showed that the particle size and morphology of HPA samples had a significant impact on the surface roughness. The HPA-1 sample, with its fine particle size and even distribution, formed a homogeneous coating that the calendering process could only slightly improve the surface roughness. However, the HPA-2 sample, with its larger and flake-shaped particles, experienced a significant reduction in surface roughness after calendering – approximately 20% in hydraulic press and 55% in roll calendering technique. The surface roughness and finishing of HPA-3 were extensively dependent on the selected calendering technique. Holding the coated separator under pressure in hydraulic press calendering could break down coarse particles into smaller ones, while roll calendering, which applies pressure for a short time, is unable to do so.

These results indicate that the calendering process is heavily dependent on the HPA particle size and morphology and can have a varying impact on surface roughness. The calendering effect is more apparent when the precursors have larger particle size and uneven particle distribution. Nevertheless, regardless of particle size and morphology, calendering can improve the particle arrangement on the surface and provide a more homogeneous surface. It is important to note that the coating pores are directly affected by particle size and morphology, as well as the coating porosity and compactness. Therefore, any change in coating porosity and compactness will affect the membrane's performance.

Figure 10 illustrates the electrolyte uptake of the coated separator both before and after calendering using various HPA particles. It is evident that the addition of a coating layer to the separator has led to an increase in electrolyte uptake. The size and morphology of the HPA particles in combination with the calendering technique is also shown to influence the electrolyte uptake and, through re-arrangement of the particles within the coating, potentially altering the surface tension.<sup>[33]</sup> While not studied here, the effects of calendering may be to either increase or decrease the uptake and is sensitive to both the coating morphology and the calendering process conditions. This, in turn, may influence the rate capability and cycling performance of the cell by increasing the lithium-ion reservoir and wettability improvement within the cell. Moreover, the results suggest that coarse-sized HPA particles may have a higher likelihood

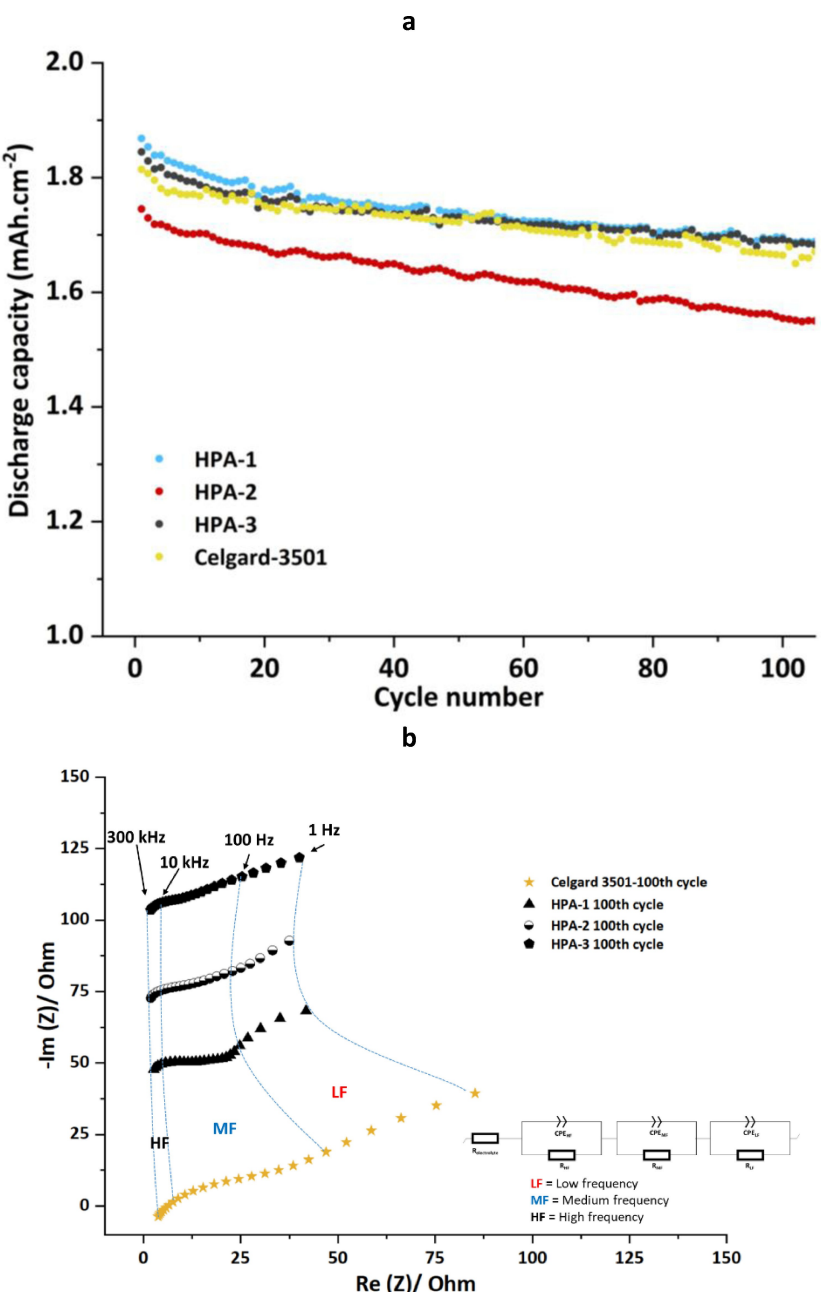


Figure 12. a) Capacity retention and b) Nyquist plot of the charged Gr|NMC811 after 100 cycles including the equivalent circuit on the right.

of storing the electrolyte inside the coating due to high porosity and thicker coating.

#### Performance in Li-ion Cell

To assess the cycling rate capability of the Gr||NMC811 (2 mAh·cm<sup>-2</sup>) full cells, the rate capability of the cells at various C-rates, ranging from a slow C-rate (C/5) to a fast C-rate (3 C) were examined, as shown in Figure 11. The impact of calendering on the cycling performance of blade-coated membranes in Li-ion batteries was also investigated using roll and hydraulic press calendering techniques.

As coated samples are performing very similar to the uncoated sample (3501), even though the thickness of the coated separators is higher. The rate capability of the coated separator was significantly affected by the calendering process, primarily due to changes in the coating's compactness and surface morphology (as seen in Figure 8 and Figure 9). Specifically, in the case of the HPA-1 sample, calendering resulted in a thinner coating with compromised porosity. This reduction in porosity can result in a loss of ion pathways and increasing tortuosity, ultimately leading to a reduced discharge capacity, particularly at higher charging rates that require a higher rate of ion transfer between electrodes.

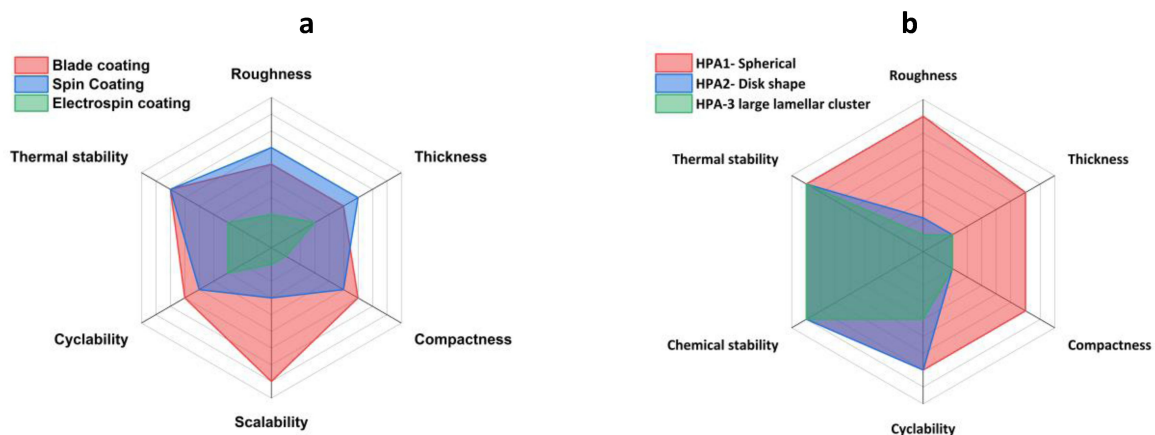


**Figure 13.** Influence of the employed coating technique (a) and HPA particle size and morphology (b) On the coating quality and performance. (Higher values are more favourable).

For the HPA-2 sample, hydraulic press calendering positively impacted the coating's thickness, compactness, and particle arrangement, while still allowing for ion pathways to exist through the pores between large particles. This resulted in an enhanced rate capability at all tested charging rates. On the other hand, roll calendering resulted in a dense coating without room for electrolyte to penetrate (as seen in Figure 8), thus compromising the ion pathways and impeding ion mobility.

The HPA-3 sample suffered from an uneven thickness and heterogeneous particle distribution on the surface, leading to poor performance at all tested charging rates. Additionally, calendering techniques were found to be unable to improve coating morphology or particle distribution, and further contributing to poor cycling performance, Hydraulic press calendering specifically.

To further evaluate the cycling performance of the HPA coated samples, long term cycling was performed on  $\text{Gr} \parallel \text{NMC811}$  (2 mAh.cm<sup>-2</sup>) full cells at C/2 (2 hours to reach to a fully charged state) (Figure 12-a). The results revealed no sign of failure in all three HPA coated samples with very similar cycling performance to benchmark sample in HPA-1 and HPA-3 samples. Whereas the HPA-3 sample obtains lower capacity and the reference sample has retained higher discharge capacity after 100 cycles. The results suggest that the reason behind the different performance in the coated separators are related to the ion mobility, the internal resistance of the cell (Figure 12-b) and electrolyte uptake of the separator (Figure 10).<sup>[34,35]</sup>

Cell stability is linked to the cell impedance (Figure 12-b), to which cell components contribute.<sup>[36]</sup> Generally, diffusive impedance dominates at low frequencies (LF), while interfacial impedance, including solid electrolyte interphase (SEI) resistance ( $R_{\text{SEI}}$ ) and charge transfer resistance ( $R_{\text{CT}}$ ), dominates at high (HF) to medium (MF) frequencies, respectively.<sup>[37]</sup> Hence, changes in LF and MF are partly attributed to surface morphology and ion diffusivity. The results suggest that adding a layer of HPA porous coating at the cathode/separator interface improves

cathode wettability, alongside enhanced ion diffusivity, by reducing cell resistance at LF and  $R_{\text{CT}}$  at MF.<sup>[34]</sup> However,  $R_{\text{SEI}}$  at HF did not show substantial changes between coated and uncoated samples using various HPA particles. Moreover, HPA-1 exhibits a more depressed EIS at the MF section, indicating a smaller  $R_{\text{CT}}$ -related semi-circle, further signifying improvement in charge transfer and ion diffusivity in the presence of HPA coating with fine particles. Therefore, coated sample with smaller particles (HPA-1 and HPA-2) obtain higher capacity due to providing homogenous charge distribution at the interface, improving the cathode wettability, and increasing the Li-ion reservoir by storing higher amount of electrolyte in the separator.

Figure 13 demonstrates the potential of using the discussed coating techniques and HPA particles to tailor a suitable alumina coating for different applications. While adding a layer of alumina improve the thermal resistance of the membranes (Figure 6), the employed coating technique results to different thickness, surface roughness and compactness that are directly influence cyclability in battery application (Figure 8, Figure 9, Figure 11 and Figure 12). Moreover, careful selection of the HPA particle size and morphology is a key factor to optimize the mentioned parameters.

## Conclusions

This study demonstrates the influence of HPA particle properties, coating techniques, and calendering on the performance of coated separators. The findings provide insights into optimizing slurry ratios, coating methods, and calendering conditions to achieve stable and high-performance coatings for various applications. Coating the separator with HPA powders was shown to improve thermal tolerance and reduce membrane shrinkage. The blade coating technique produced coatings with smooth surfaces and suitable thickness, while electro-spin coating resulted in unfavorable agglomeration of particles and stranded binder.

HPA-coated separators had minimal impact on the stability of the electrolyte and did not induce or accelerate electrolyte decomposition. Calendering affected the surface morphology, roughness, and compactness of the HPA coating, with the particle size and morphology of HPA samples playing a significant role in surface roughness. As expected, coating the separator with HPA particles increases the electrolyte uptake. The rate capability of the coated separators in Li-ion batteries was significantly affected by the calendering process, primarily due to changes in coating compactness and surface morphology. The long-term cycling performance coupled with EIS results, suggested an interconnection between the cells' cycling performance and internal cell resistance. Adding a coating layer to the separator reduces resistance at low and medium frequencies, attributed to improved cathode wetting and reduced charge transfer. Overall, these findings contribute to the understanding of coated separator performance and offer valuable guidance for the design and optimization of coated separators for diverse applications.

## Acknowledgements

This project is funded by the Future Battery Industries Cooperative Research Centre as part of the Commonwealth Cooperative Research Centre Program. The authors gratefully acknowledge the Office of the Deputy Vice-Chancellor of Research of Deakin University for funding of this research through the Battery Technology Research and Innovation Hub (BatTRI-Hub). Open Access publishing facilitated by Deakin University, as part of the Wiley - Deakin University agreement via the Council of Australian University Librarians.

## Conflict of Interests

The authors declare no conflict of interest.

## Data Availability Statement

The data that support the findings of this study are available from the corresponding author upon reasonable request.

**Keywords:** Alumina · Ceramic · Coating · Separator · Lithium-ion batteries

- [1] Z. He, Z. Lyu, Q. Gu, L. Zhang, J. Wang, *Colloids Surf. A* **2019**, 578, 123513.
- [2] N. Gao, Z.-K. Xu, *Sep. Purif. Technol.* **2019**, 212, 737–746.

- [3] C. Zhu, Y. Su, D. Zhang, Q. Ouyang, *Mater. Sci. Eng. A* **2020**, 793, 139839.
- [4] L. Velleman, G. Triani, P. J. Evans, J. G. Shapter, D. Losic, *Microporous Mesoporous Mater.* **2009**, 126, 87–94.
- [5] X. Huang, R. He, M. Li, M. O. L. Chee, P. Dong, J. Lu, *Mater. Today* **2020**, 41, 143–155.
- [6] M. Eftekharinia, M. Hasanpoor, M. Forsyth, R. Kerr, P. C. Howlett, *ACS Appl. Energ. Mater.* **2019**, 2, 6655–6663.
- [7] Z. Yuan, N. Xue, J. Xie, R. Xu, C. Lei, *J. Electrochem. Soc.* **2021**, 168, 030506.
- [8] D. Parikh, C. J. Jafta, B. P. Thapaliya, J. Sharma, H. M. Meyer, C. Silkowski, J. Li, *J. Power Sources* **2021**, 507, 230259.
- [9] J. Choi, P. J. Kim, *Curr. Opin. Electrochem.* **2022**, 31, 100858.
- [10] D. H. Jeon, J.-H. Song, J. Yun, J.-W. Lee, *ACS Nano* **2022**, 17.2, 1305–1314..
- [11] X. Shi, Q. Sun, B. Boateng, Y. Niu, Y. Han, W. Lv, W. He, *J. Power Sources* **2019**, 414, 225–232.
- [12] D. V. Carvalho, N. Loeffler, G.-T. Kim, S. Passerini, *Membranes* **2015**, 5, 632–645.
- [13] J. Zhang, Z. Liu, Q. Kong, C. Zhang, S. Pang, L. Yue, X. Wang, J. Yao, G. Cui, *ACS Appl. Mater. Interfaces* **2013**, 5, 128–134.
- [14] X. Jiang, X. Zhu, X. Ai, H. Yang, Y. Cao, *Applied Materials & Interfaces* **2017**, 9, 25970–25975.
- [15] W. Chen, Y. Liu, Y. Ma, W. Yang, *J. Power Sources* **2015**, 273, 1127–1135.
- [16] S. J. Cho, H. Choi, J. H. Youk, *Fibers Polym.* **2020**, 21, 993–998.
- [17] M. Abdollahifar, H. Cavers, S. Scheffler, A. Diener, M. Lippke, A. Kwade, *Energy Materials* **2023**, 2300973.
- [18] W. Haselrieder, S. Ivanov, D. K. Christen, H. Bockholt, A. Kwade, *ECS Trans.* **2013**, 50, 59.
- [19] W. Yi, Z. Huaiyu, H. Jian, L. Yun, Z. Shushu, *J. Power Sources* **2009**, 189, 616–619.
- [20] J. Wang, X. Bokhimi, A. Morales, O. Novaro, T. Lopez, R. Gomez, *J. Phys. Chem. B* **1999**, 103, 299–303.
- [21] C. V. Chandran, C. E. A. Kirschhock, S. Radhakrishnan, F. Taulelle, J. A. Martens, E. Breynaert, *Chem. Soc. Rev.* **2019**, 48, 134–156.
- [22] L. A. O'Dell, S. L. Savin, A. V. Chadwick, M. E. Smith, *Solid State Nucl. Magn. Reson.* **2007**, 31, 169–173.
- [23] V. Wenzel, H. Nirschl, D. Nötzel, *Energy Technol.* **2015**, 3, 692–698.
- [24] K. S. Reddy, V. S. Reddy, J. Sujitha, M. Pydimalla, *Techniques and Innovation in Engineering Research* **2022**, 6, 129–152.
- [25] M. Hasanpoor, M. Eftekharinia, T. Pathirana, U. Pal, R. Kerr, M. Forsyth, P. C. Howlett, *ACS Appl. Energ. Mater.* **2021**, 4, 6310–6323.
- [26] M. Kim, J. H. Park, *J. Power Sources* **2012**, 212, 22–27.
- [27] C. Meyer, H. Bockholt, W. Haselrieder, A. Kwade, *J. Mater. Process. Technol.* **2017**, 249, 172–178.
- [28] C. Yang, H. Tong, C. Luo, S. Yuan, G. Chen, Y. Yang, *J. Power Sources* **2017**, 348, 80–86.
- [29] C. Peabody, C. B. Arnold, *J. Power Sources* **2011**, 196(19), 8147–8153.
- [30] Z. Zhang, Y. Lai, Z. Zhang, K. Zhang, J. Li, *Electrochim. Acta* **2014**, 129, 55–61.
- [31] W. Chen, L. Shi, Z. Wang, J. Zhu, H. Yang, X. Mao, M. Chi, L. Sun, S. Yuan, *Carbohydr. Polym.* **2016**, 147, 517–524.
- [32] A. Davoodabadi, J. Li, Y. Liang, R. Wang, H. Zhou, D. L. Wood, T. J. Singler, C. Jin, *J. Electrochem. Soc.* **2018**, 165, A2493.
- [33] C. Shi, P. Zhang, L. Chen, P. Yang, J. Zhao, *J. Power Sources* **2014**, 270, 547–553.
- [34] E. Shekarian, M. R. Jafari Nasr, T. Mohammadi, O. Bakhtiari, M. Javanbakht, *Journal of Nanostructures* **2019**, 9, 736–750.
- [35] R. Xu, H. Huang, Z. Tian, J. Xie, C. Lei, *Polymer* **2020**, 12, 117.
- [36] P. Vadhra, J. Hu, M. J. Johnson, R. Stocker, M. Braglia, D. J. L. Brett, A. J. E. Rettie, *ChemElectroChem* **2021**, 8, 1930–1947.
- [37] S. Wang, J. Zhang, O. Gharbi, V. Vivier, M. Gao, M. E. Orazem, *Nature Reviews Methods Primers* **2021**, 1, 41.

Manuscript received: April 4, 2024  
Revised manuscript received: May 13, 2024  
Accepted manuscript online: May 21, 2024  
Version of record online: July 5, 2024